Supplementary materials for

ENSO teleconnection to interannual variability in carbon monoxide over the North Atlantic European region in spring

Yi Liu[1], Jane Liu[2,3*], Min Xie[1], Keyan Fang[3], David W. Tarasick[4], Honglei Wang[2,5], Lingyun Meng[6], Xugeng Cheng[3], Han Han[7], Xun Zhang[6]

[1]School of Atmospheric Sciences, Nanjing University, Nanjing, China
[2]Department of Geography and Planning, University of Toronto, Toronto, Canada
[3]Laboratory for Humid Subtropical Eco-Geographical Processes of the Ministry of Education, School of Geographical Sciences, Fujian Normal University, Fuzhou, China
[4]Air Quality Research Division, Environment and Climate Change Canada, Downsview, Canada
[5]Key Laboratory for Aerosol-Cloud-Precipitation of the China Meteorological Administration, Nanjing University of Information Science & Technology, Nanjing, China
[6]International Institute for Earth System Science, Nanjing University, Nanjing, China
[7]Laboratory for Climate and Ocean-Atmosphere Studies, Department of Atmospheric and Oceanic Sciences, School of Physics, Peking University, Beijing, China

***Correspondence:**
Jane Liu
janejj.liu@utoronto.ca

S1 Description of MOPITT satellite data

MOPITT (Measurements Of Pollution In The Troposphere) is the first satellite instrument launched by NASA to continuously measure tropospheric carbon monoxide. MOPITT has been aboard the Terra satellite since 1999, and officially began measurements in March 2000, using near-infrared at 2.3 μm and thermal-infrared radiation at 4.7 μm. MOPITT views the Earth at a spatial resolution of 22 km by 22 km and measures a near-global distribution of CO every 3 days. We use MOPITT monthly mean data (MOP03JM, level 3, version 9, Deeter et al., 2022) with a horizontal resolution of 1°x1° (latitude, longitude). To improve data quality, only daytime data with signal degrees of freedom greater than 0.75 are utilized in the study.

Reference

Deeter, M., Francis, G., Gille, J., Mao, D., Martínez-Alonso, S., Worden, H., et al. (2022). The MOPITT Version 9 CO product: sampling enhancements and validation. Atmos. Meas. Tech. 15(8), 2325-2344. doi: 10.5194/amt-15-2325-2022.

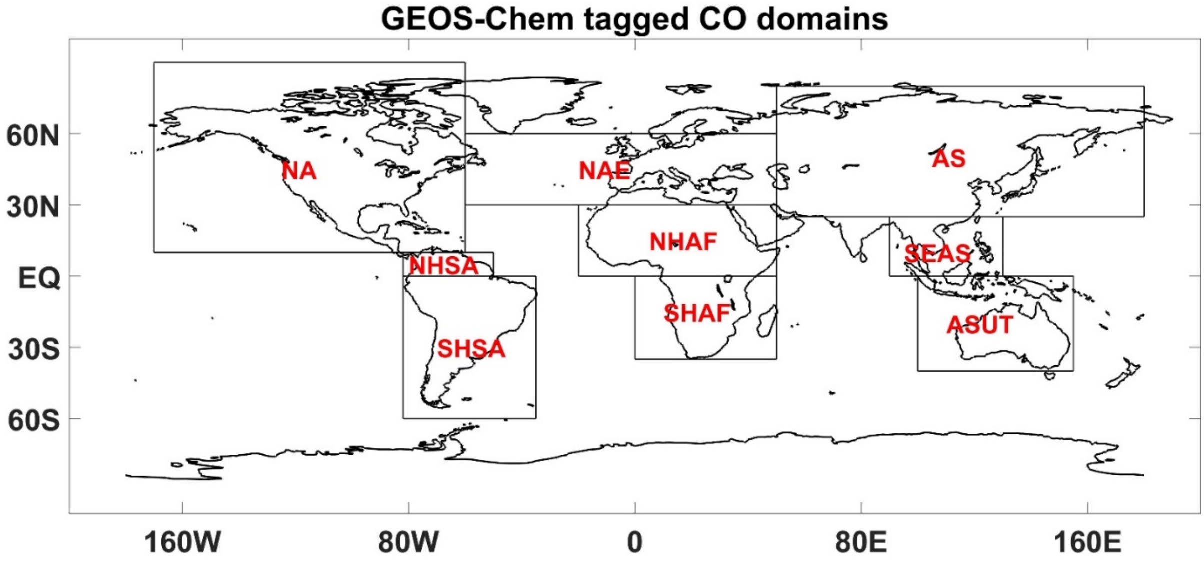

Figure S1: Domains defined in the GEOS-Chem tagged CO simulation.

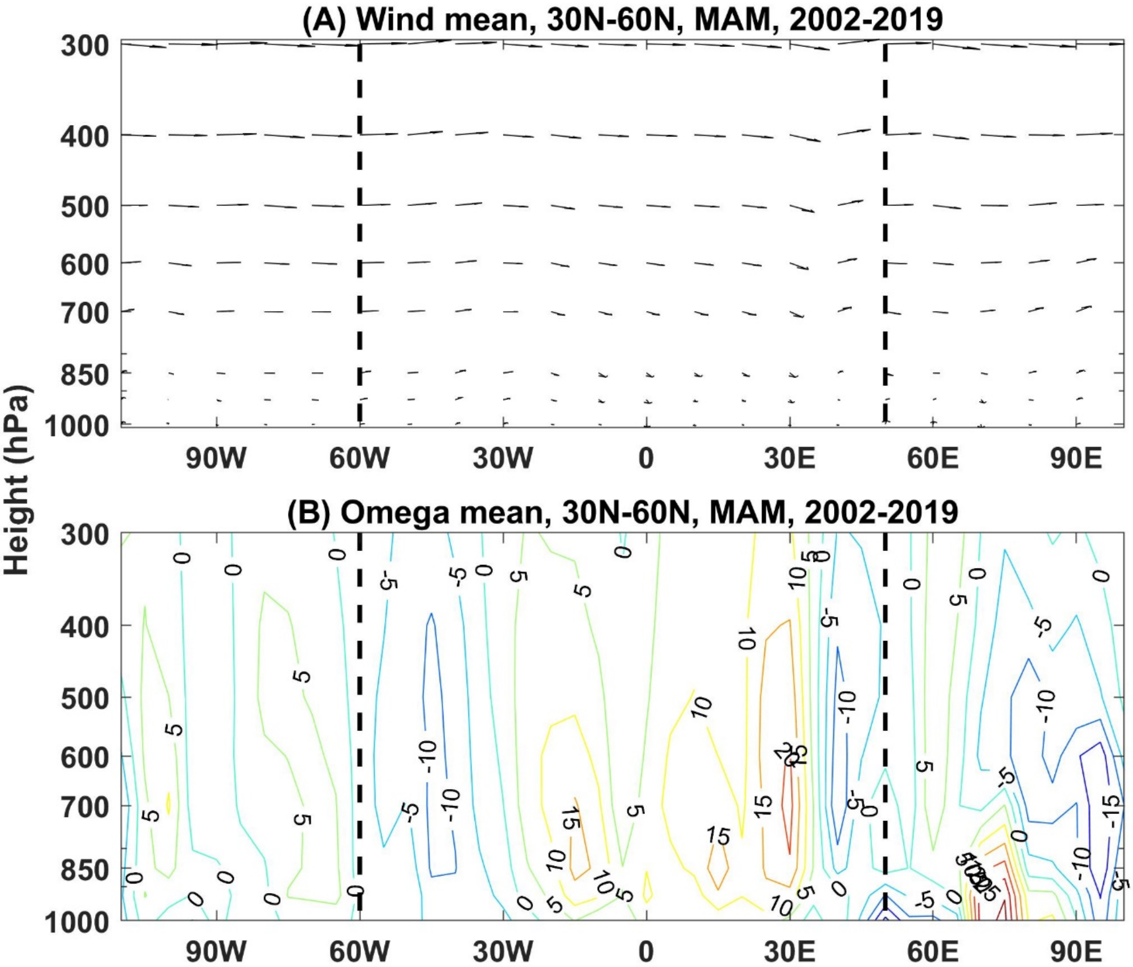

Figure S2: (A) The longitude-altitude cross section of wind fields averaged over 30°N-60°N, MAM, 2002-2019. (B) The longitude-altitude across section of vertical velocity omega (Pa s^{-1}) averaged over 30°N-60°N, MAM, 2002-2019. The vertical wind velocity in Figures S2A and S2B is enlarged by 1000 times for illustration purposes. The vertical dashed lines indicate longitudinal borders of the NAE.

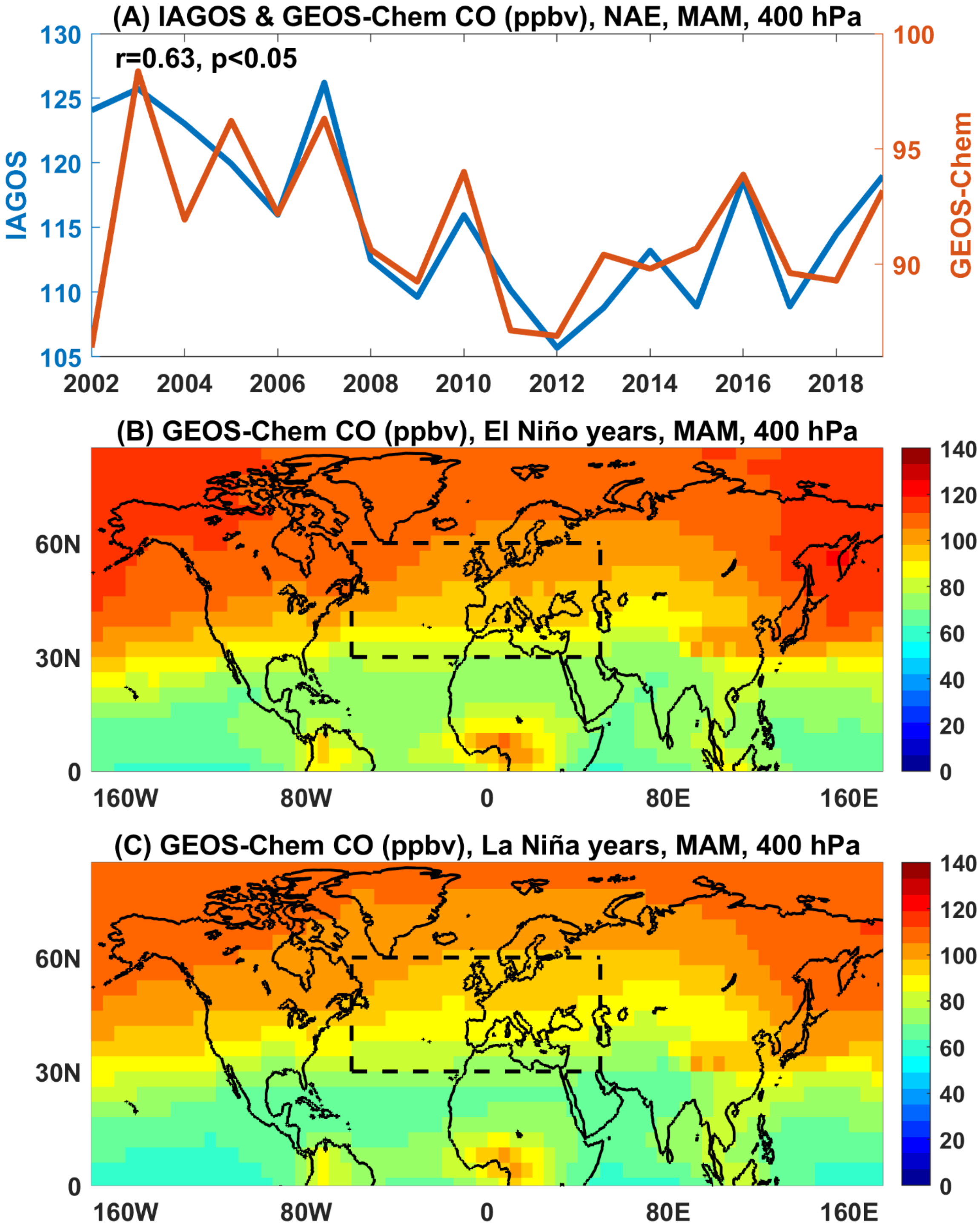

Figure S3: (A) IAV in MAM CO_{DT} concentrations (blue line) over the NAE based on the trajectory-mapped IAGOS data (blue line) and the GEOS-Chem simulations from full chemistry run (brown line). The correlation coefficient (*r*) between the two series and its p-value (*p*) are also shown. (B) The seasonal mean CO distribution in March, April, and May at 400 hPa in El Niño years. The dashed lines indicate the North Atlantic European region (NAE). (C) The same as (B), but in La Niña years.

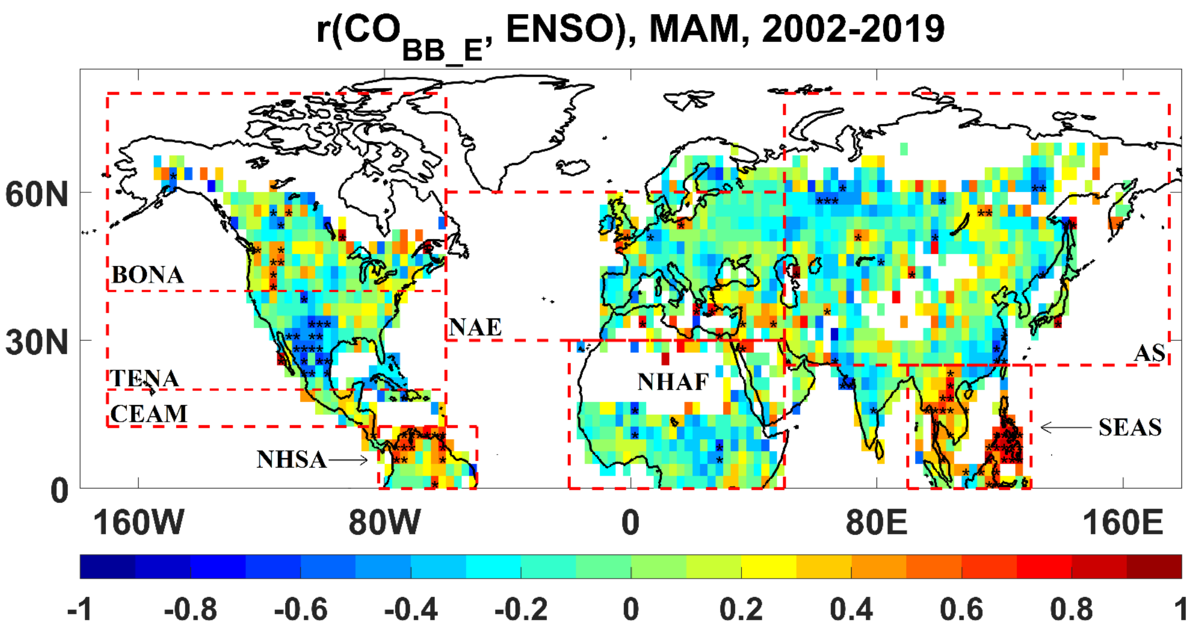

Figure S4: Correlation coefficients between the ENSO index and CO emissions from biomass burning (CO_{BB_E}) over 2002-2019, with asterisks indicating the 95% significance level. The emission values are based on GFED4.1s data.

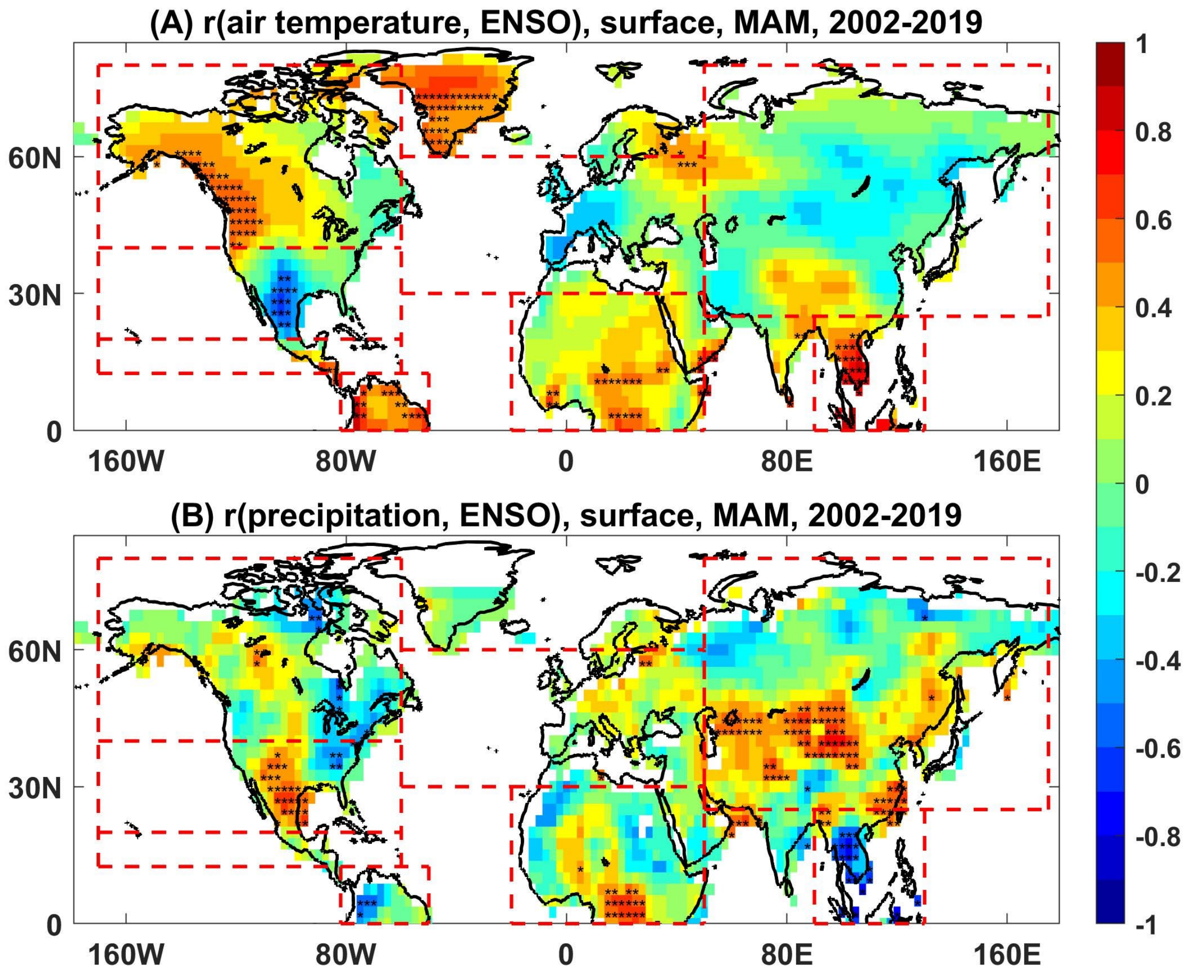

Figure S5: (A) Correlation coefficient between the ENSO index and surface air temperature in MAM over 2002-2019, with asterisks indicating the 95% significance level. (B) The same as (A), but for surface precipitation.

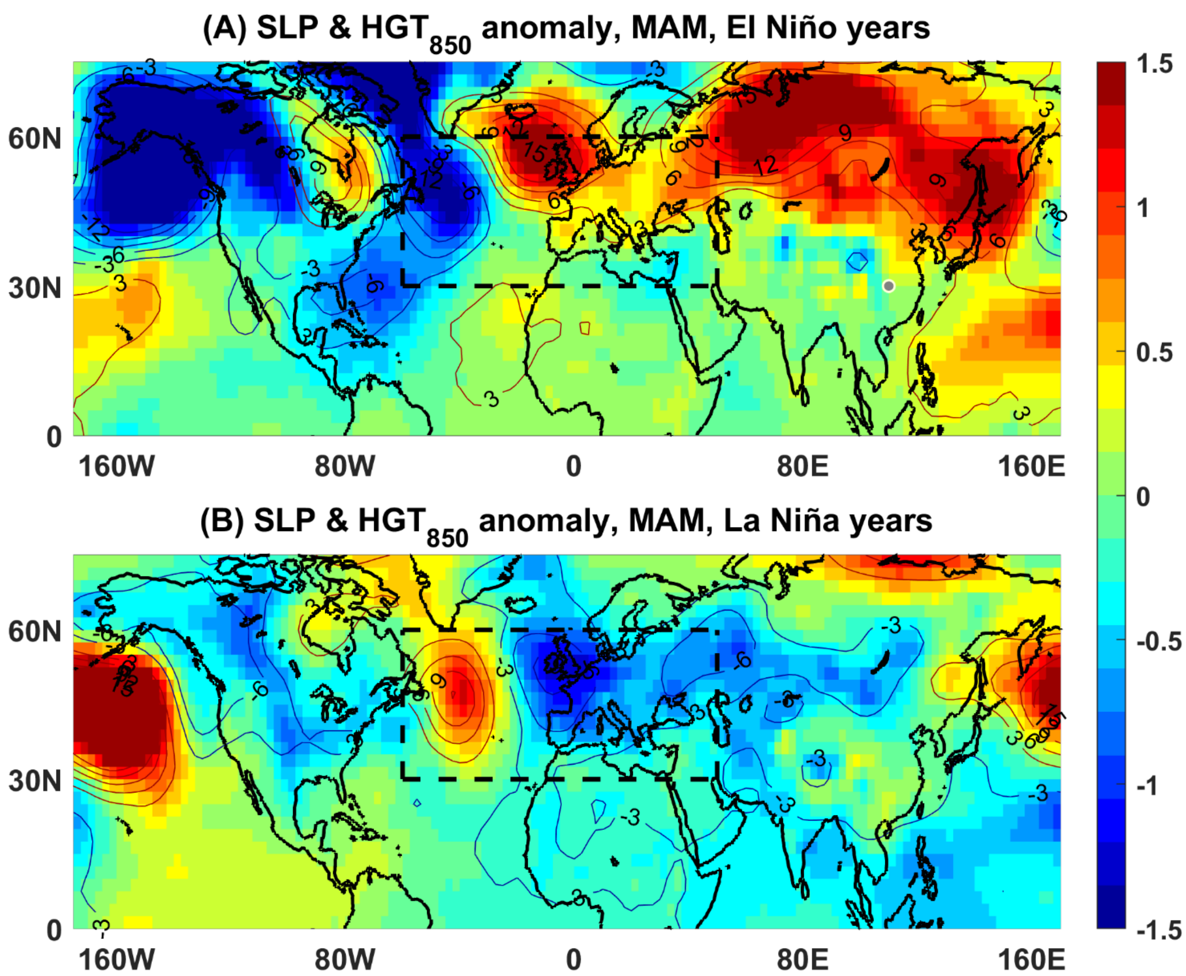

Figure S6: (A) The differences in MAM sea level pressure (SLP, in color, unit: hPa) and geopotential height at 850 hPa (HGT, in contour, unit: m) between El Niño years and the 18-year mean. (B) The same as (A), but for the differences between La Niña years and the mean.

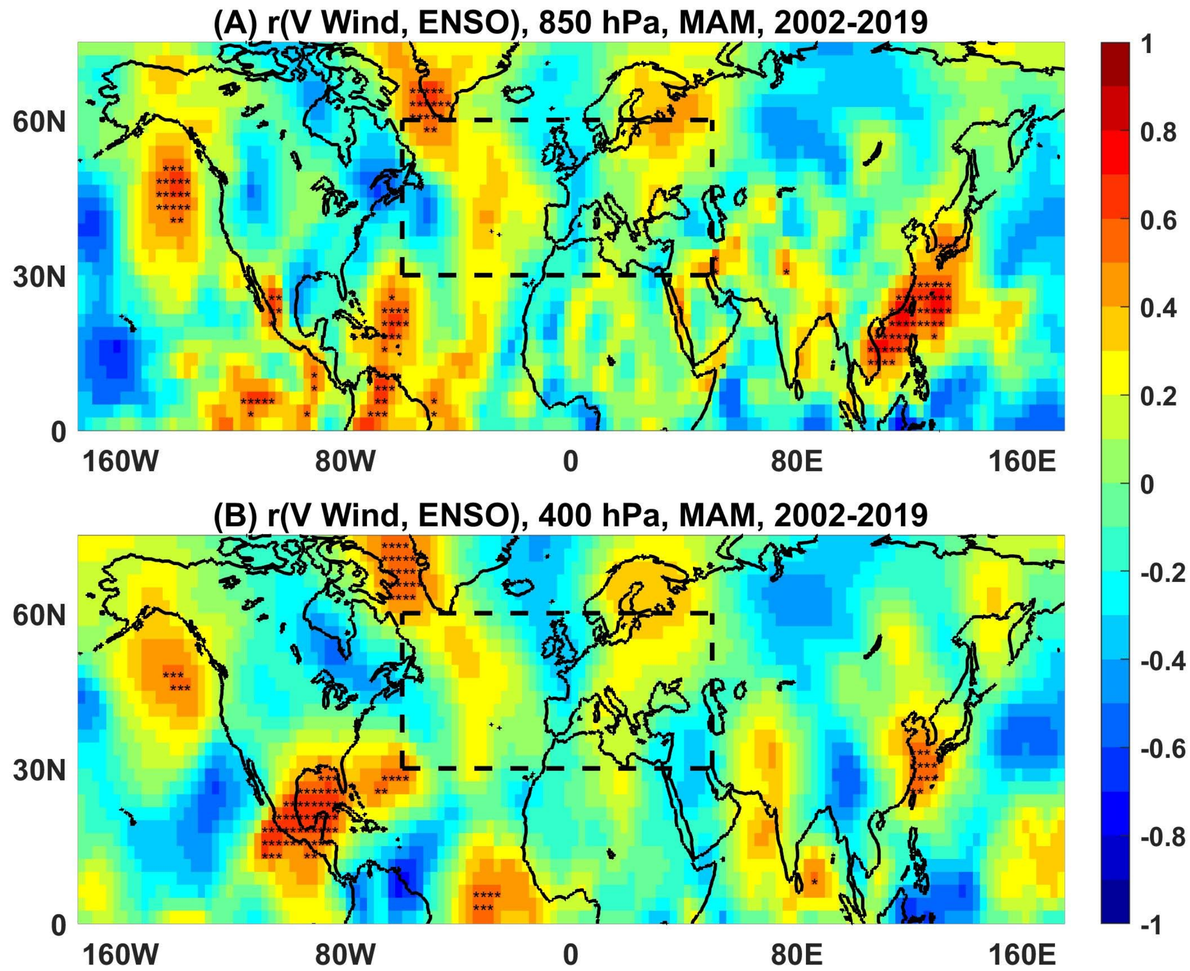

Figure S7: (A) Correlation coefficient between the ENSO index and wind in the V direction at 850 hPa in MAM over 2002-2019, with asterisks indicating the 95% significance level. (B) the same as (A), but at 400 hPa.

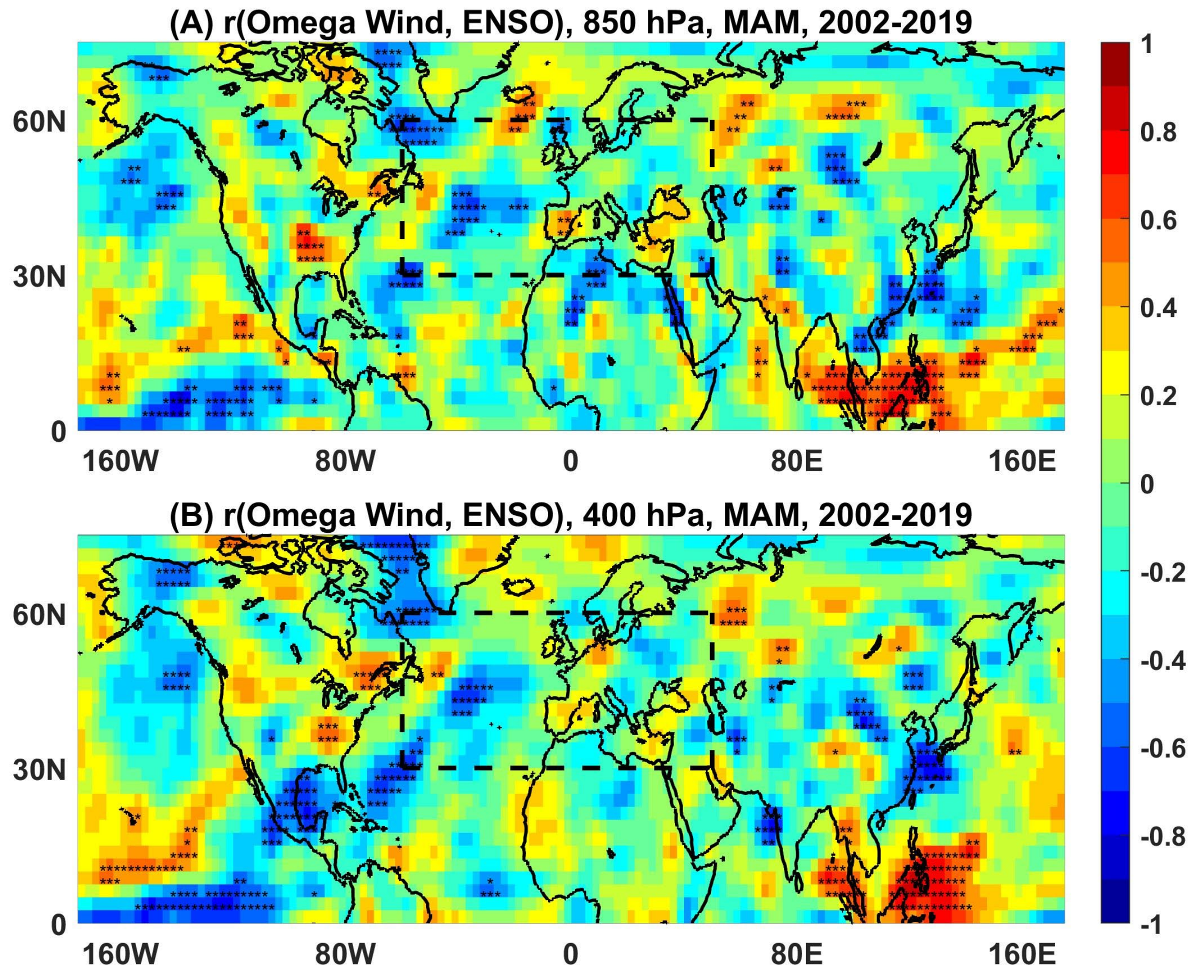

Figure S8: The same as Figure S7, but for vertical velocity (ω).

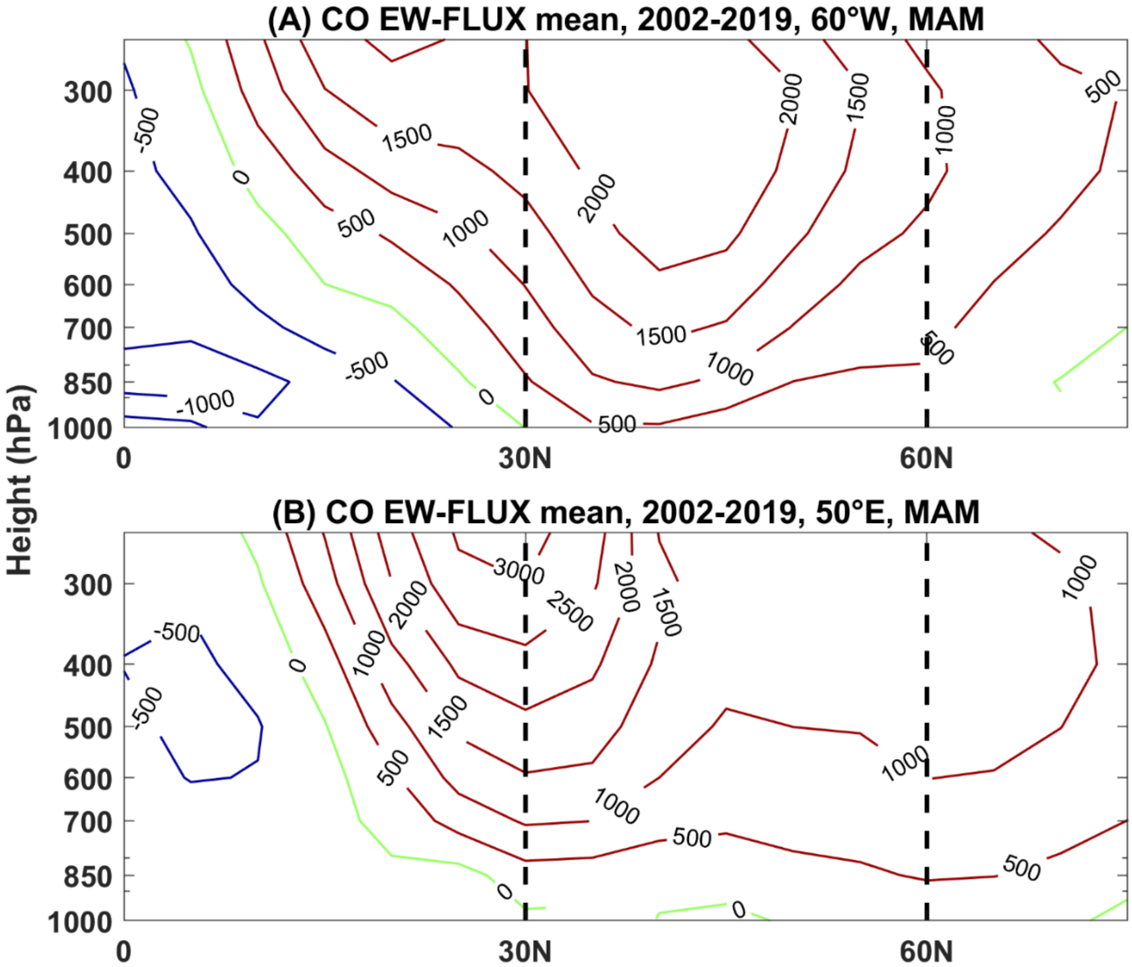

Figure S9: (A) The latitude-altitude cross section of mean east-west horizontal CO flux (in ppbv m s^{-1}) at the west border of the NAE (60°W) in MAM, averaged over 2002-2019. (B) The same as (A), but at the east border of the NAE (50°E). Eastward flux is positive. The vertical lines at 30°N and 60°N show the latitudinal borders of the NAE.

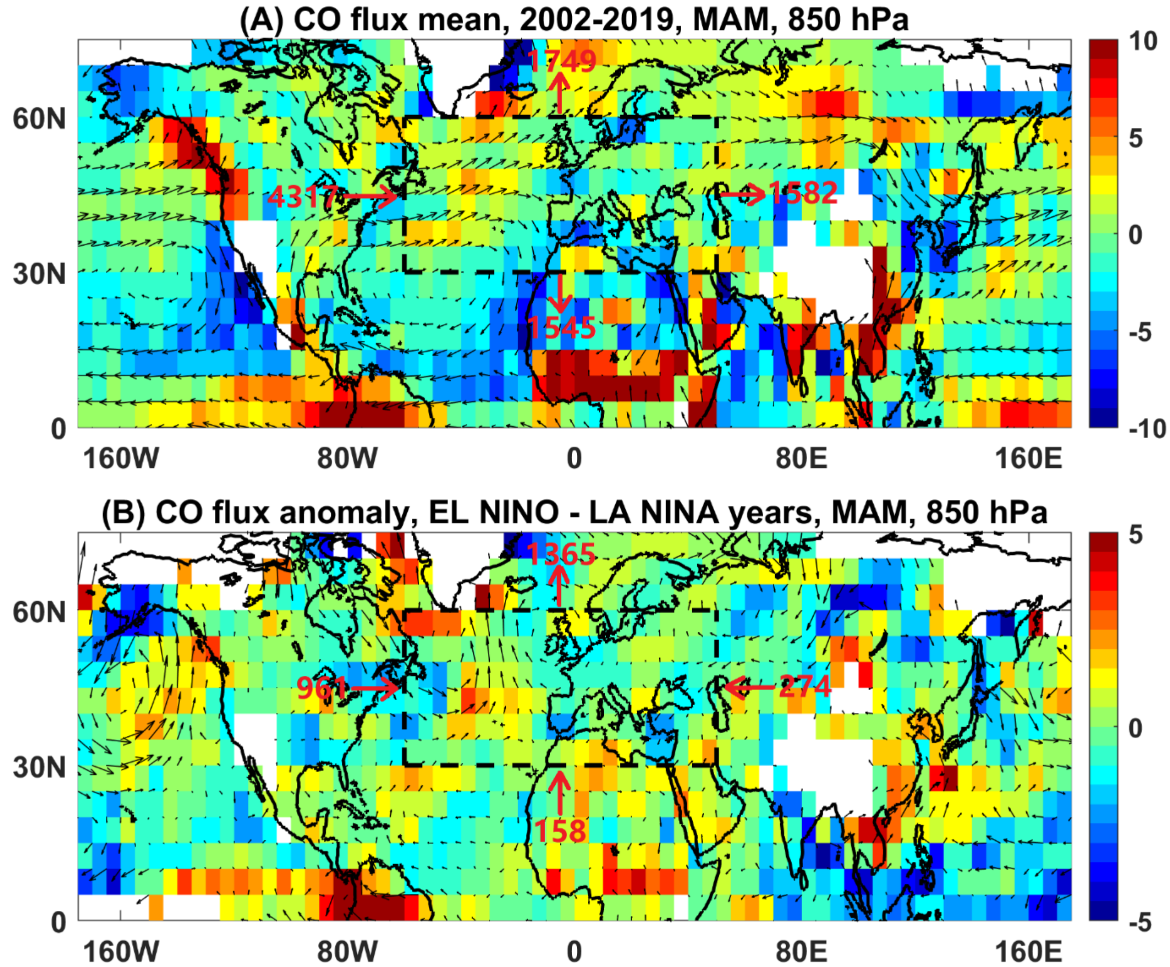

Figure S10: (A) The mean of horizontal CO flux fields (arrows, ppbv m s^{-1}) averaged over 2002-2019 MAM at 850 hPa. Overlaid is the corresponding vertical CO flux fields (in color, -ppbv Pa s^{-1}). (B) The difference in horizontal CO flux field (arrows, ppbv m s^{-1}) between El Niño and La Niña years in MAM at 850 hPa. Overlaid is the corresponding difference in vertical CO flux (in color, -ppbv Pa s^{-1}). The white areas are missing values, mostly due to topography (high elevation). Note that the upward flux is positive.

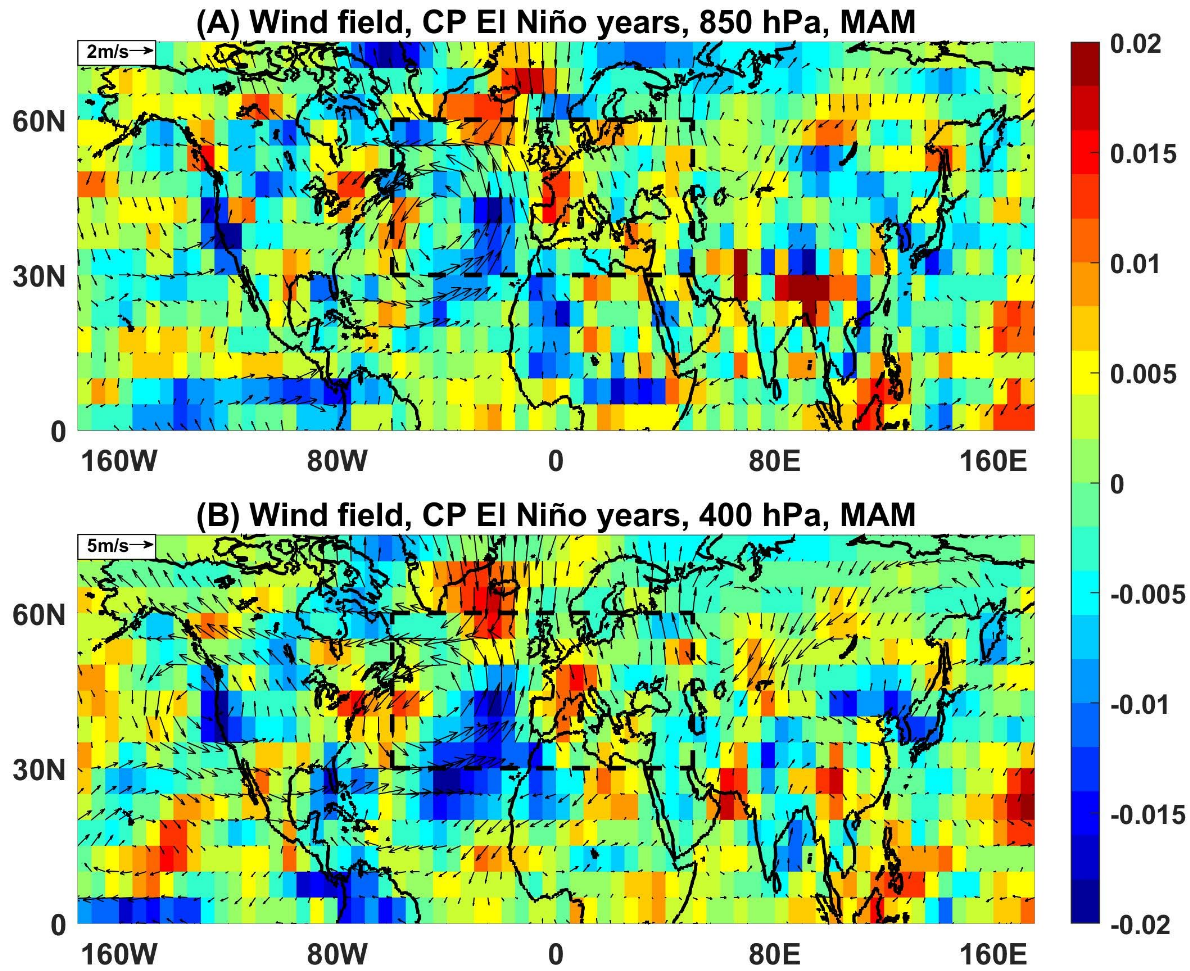

Figure S11: (A) Difference in horizontal wind (arrows) between CP El Niño years and the mean in MAM at 850 hPa. Overlaid is the corresponding difference in vertical velocity (in color, Pa s^{-1}). (B) The same as (A), but at 400 hPa. Note the upward velocity is negative (in blue).

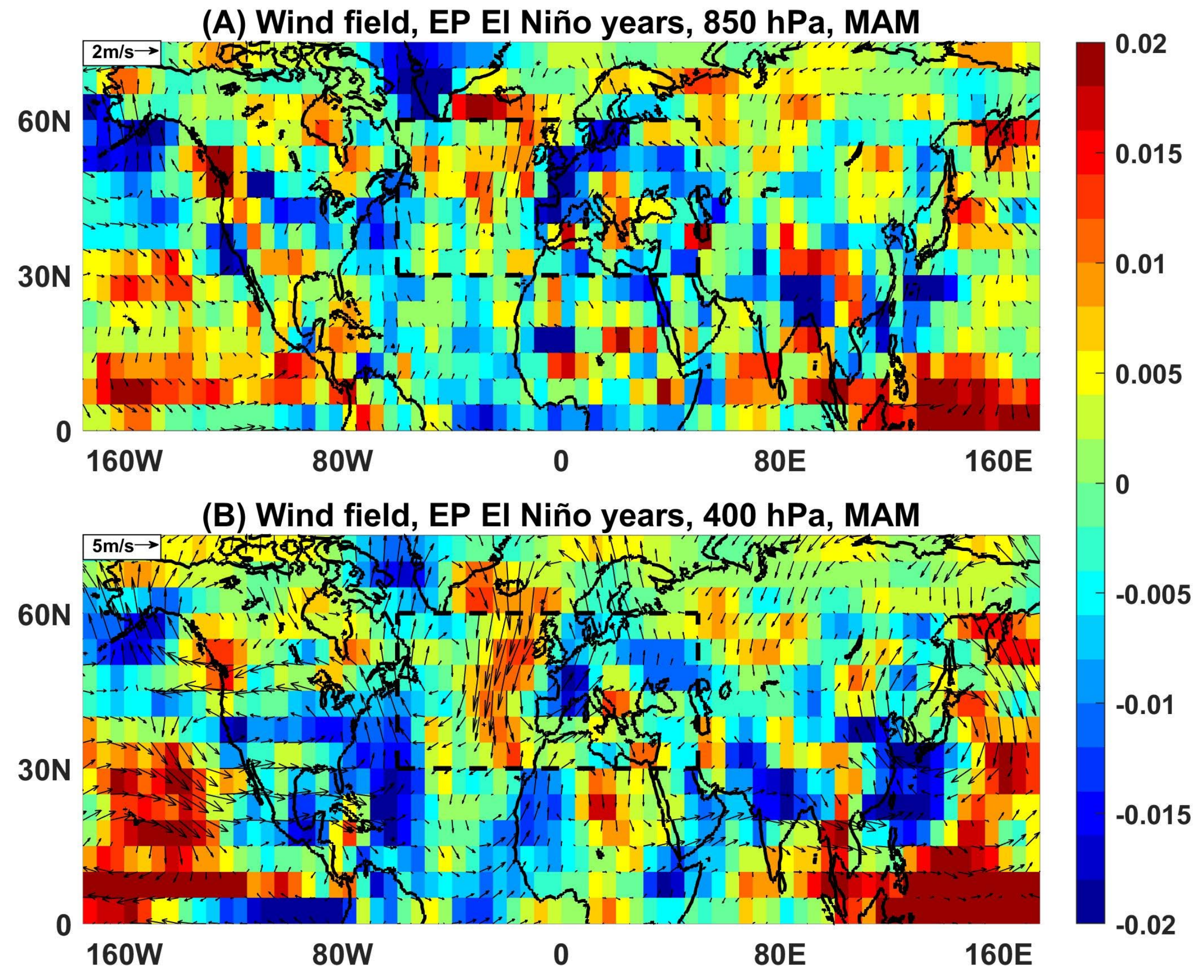

Figure S12: The same as Figure S11, but the difference between EP El Niño years and the mean.

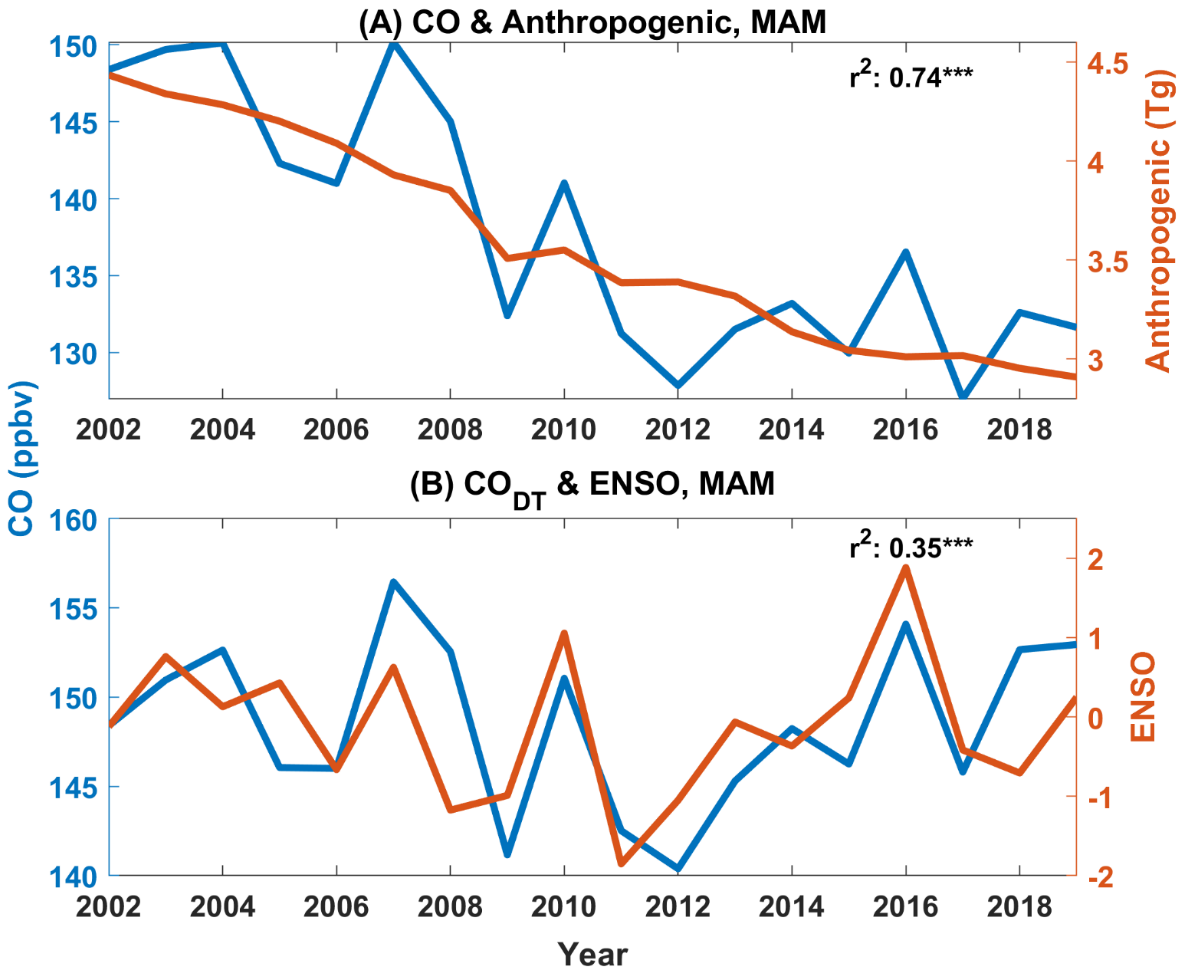

Figure S13: (A) CO concentrations at 850 hPa (blue line) and anthropogenic emissions (brown line) over the NAE in MAM from 2002 to 2019. "***" indicates that the linear correlation is at the 99% significance level ($p<0.01$). (B) The same as (A), but for detrended CO concentrations (CO_{DT}) at 850 hPa (blue line) and the corresponding ENSO index (brown line).

Table S1: Correlation coefficients (r) between the ENSO index and detrended CO concentrations in MOPITT and GEOS-Chem simulations, averaged over the NAE at different altitudes.

Altitude (hPa)	**r (MOPITT CO_{DT_NAE}, ENSO)**	**r (GEOS-Chem CO_{DT_NAE}, ENSO)**
200	0.52**	0.81***
300	0.52**	0.74**
400	0.60***	0.73**
500	0.67***	0.73**
600	0.72***	0.73**
700	0.74***	0.72**
800	0.73***	0.67**
900	0.68***	0.63**

"**" indicates that r is statistically significant at the 95% level ($p<0.05$) and "***" at the 99% level ($p<0.01$).

Table S2: (A) GEOS-Chem simulations of fire-induced CO components from different regions over the NAE (CO_{BB_NAE}, ppbv) at 400 hPa. The correlation coefficient (*r*) between the ENSO index and CO_{BB_NAE} is also shown. (B) The same as (A), but for CO over the different source regions (CO_{BB_source}, ppbv). See Figure S1 for the region definition.

(A) Fire-induced CO in the North Atlantic European region (NAE), 400 hPa

From Region	CO_{BB_NAE} (ppbv)	r (CO_{BB_NAE}, ENSO)
NHSA	0.17	0.67**
SEAS	1.17	0.38
NA	2.24	0.29
AS	2.44	-0.09
NAE	0.74	0.02
NHAF	3.77	-0.27
NA+NHSA+SEAS	3.58	0.43*

(B) Fire-induced CO in different source regions, 400 hPa

In Region	CO_{BB_source} (ppbv)	r (CO_{BB_source}, ENSO)
NHSA	1.64	0.33
SEAS	2.38	0.26
NA	1.82	0.31
AS	3.96	0.02
NHAF	9.69	-0.25
NA+NHSA+SEAS	1.88	0.37

"*" indicates that *r* is at the 90% significance level ($p<0.10$), "**" at the 95% level ($p<0.05$).

Table S3. GEOS-Chem simulated CO concentrations in the NAE and the associated partition from CO sources from different regions at 850 hPa and 400 hPa. By region, the CO sources include emissions from biomass burning, biofuel, and anthropogenic activities from each of the defined regions. The remainder of CO sources are included in "Other sources". "ROW" denotes the region of "the rest of the world". See Figure S1 for the region definition. "ΔCO" is the difference in CO concentrations between El Nino and La Nina years.

	CO at 850 hPa				CO at 400 hPa			
Region	**Mean (ppbv)**	**El Nino Anomaly (ppbv)**	**La Nina Anomaly (ppbv)**	**ΔCO /mean (%)**	**Mean (ppbv)**	**El Nino Anomaly (ppbv)**	**La Nina Anomaly (ppbv)**	**ΔCO /mean (%)**
AS	30.71	1.13	-0.01	3.68	26.86	1.31	-0.12	4.88
NAE	17.27	0.64	-0.67	3.71	5.65	0.09	-0.09	1.59
NA	17.09	1.11	-0.65	6.50	10.53	0.66	-0.31	6.27
NHAF	6.61	-0.62	0.34	-9.38	5.6	-0.59	0.25	-10.54
SEAS	3.84	0.93	-0.26	24.22	3.03	0.64	-0.16	21.12
NHSA	0.49	0.19	-0.08	38.78	0.37	0.12	-0.05	32.43
AUST	0.58	0.08	-0.08	13.79	0.46	0.11	-0.09	23.91
SHSA	0.53	0.05	0.01	9.43	0.47	0.05	0.00	10.64
SHAF	0.6	0.06	-0.01	10.00	0.49	0.05	0.00	10.20
ROW	0.47	0.01	0.00	2.13	0.25	0.01	0.00	4.00
Other sources	31.59	-1.08	0.27	-3.42	35.77	-0.4	-0.27	-1.12
Total	109.78	2.5	-1.14	2.28	89.48	2.05	-0.84	2.29